Full title: Substrate traits shape the structure of microbial community engaged in metabolic division of labor

Running title: Substrate traits shape community structure

Miaoxiao Wang[1, 2, 3, 4], Xiaoli Chen[1, 5], Yue-Qin Tang[4], Yong Nie[1#] and Xiao-Lei Wu[1, 5, 6#]

[1] College of Engineering, Peking University, Beijing 100871, China

[2] Department of Environmental Systems Science, ETH Zurich, Zurich, Switzerland

[3] Department of Environmental Microbiology, Eawag, Dübendorf, Switzerland

[4] College of Architecture and Environment, Sichuan University, Chengdu, China

[5] Institute of Ocean Research, Peking University, Beijing 100871, China

[6] Institute of Ecology, Peking University, Beijing 100871, China

[#]Corresponding author: Research Scientist, College of Engineering, Peking University.

Tel: +86 10-62759047; Fax: +86 10-62759047; E-mail: nieyong@pku.edu.cn

[#]Corresponding author: Professor, College of Engineering, Peking University.

Tel: +86 10-62759047; Fax: +86 10-62759047; E-mail: xiaolei_wu@pku.edu.cn

Abstract

Metabolic division of labor (MDOL) is widespread in nature, whereby a complex metabolic pathway is shared between different strains within a community for mutual benefit. However, little is known about how the mutual interactions in the microbial community engaged in MDOL are regulated. We hypothesized that when degradation of an organic compound is carried out via MDOL, the substrate traits (i.e., concentration and its toxicity) modulate the benefit allocation between the two microbial populations, thus affecting the structure of this community. We tested this hypothesis by combining mathematical modelling with experiments using engineered synthetic microbial consortia. Numerous modelling analyses suggested that the proportion of the population executing the first metabolic step can be simply estimated by Monod-like formulas governed by substrate traits. The model and the proposed formula quantitatively predicted the structure of our synthetic consortia composed of two strains degrading salicylate through MDOL. Individual-based modelling and colony pattern formation assays further indicated that our rule is also applicable to estimating community structure in spatially structured environments. Our results demonstrate that the structure of the microbial communities can be quantitatively predicted from simple environmental factors, such as substrate concentration and its toxicity, which provides novel perspectives on understanding the assembly of natural communities, as well as insights into how to manage artificial microbial systems.

Introduction

In natural environments, microorganisms rarely live autonomously; instead, they interact with other individuals to form complex communities, in which they secrete a variety of toxins to compete with each other, or share metabolites to mutually benefit their survival. Among diverse modes of microbial interaction, metabolic division of labor (MDOL) is one of the most widespread phenomena, where distinct populations perform different but complementary steps of the same metabolic pathway [1-4]. MDOL controls numerous ecologically and environmentally important biochemical processes. One important aspect of microbial metabolism implemented by MDOL is the degradation of a variety of complex organic compounds, including PAHs [5, 6], pesticide [7-10], plastics [11], antibiotics [12], or polysaccharides [13, 14]. Bacterial degradation of these complex substrates is usually mediated by long metabolic pathways via a number of intermediates. While these pathways often remain intact within one population, they are frequently found segregated across different members within a community in a MDOL manner. Typical examples include syringate degradation via sequential cross-feeding between *Acetobacterium woodii* and *Pelobacter acidigallici* [5], phenanthrene degradation between *Marinobacter* sp. N4 and other PAH-degrading microbes in marine environments [6], as well as atrazine degradation through MDOL within four bacterial species [9]. However, little is known about how microbial communities engaged in MDOL are regulated [15].

The substrate whose concentration spatially and temporally fluctuates in the marine [16], soil [17] and wastewater [18] environments, acts as one of the most important

conditions that govern the performance of the microbial communities [19-21]. Firstly, the concentration of substrates regulates the growth of microbial populations according to the Monod equation [22]. Secondly, many substrates such as PAHs [23, 24], pesticide [7-10], and antibiotics [12], are toxic to bacterial cells, inhibiting their growth. Increasing substrate concentration enhances resource availability of a population that benefit its growth, but also potentially increases the toxic effects of substrate that harms its growth (e.g., growth kinetics may follow the equations integrated with toxic terms [25]). Thus, concentration and toxicity of substrate profoundly affect the fitness of its microbial degraders [24, 26, 27]. However, it still remains ill-defined how substrate straits affect the relative fitness of different strains involved in a community, and thus govern the structure of the community. As structure of a community is fundamental to determine its functioning [28, 29], revealing this question is fundamental for managing such microbial systems for the removal of serious pollutants.

Distinct from the pure culture, the effects of substrate on different populations involved in a MDOL community may vary quite a lot. Firstly, asymmetric benefit allocation exists between different populations in the MDOL community. In MDOL communities that degrade organic compounds, only the population performing the last steps can produce the growth resources (such as small organic acids) that support the bacterial growth (Supplementary Figure 1). Therefore, the population performing the last steps can preferentially acquire and privatize these nutrients (which we henceforth call *product privatization*), thus acquiring the greater benefit, while the other members

have to collect nutrients leaked from this population (Figure 1; left of the first row). This uneven allocation of limited resources generally benefits the population that executes the last steps (we henceforth named this population the 'Embezzler', analogous to a human worker responsible for the final step of an assembly line, who pockets the final product and fails to share profits with other workers). This phenomenon has been observed in many recent studies [7, 10, 30]. Increasing substrate concentration would enhance the flux of metabolites [31, 32]. Because the Embezzler only have a limited capacity of consuming the final product, increased metabolic flux causes more product released from the Embezzler cells, in turn facilitating the growth of the other population (Figure 1; Right of the first row). Secondly, substrate toxicity exerts different influences on different members. The population performing the first step transforms the toxic substrate to the intermediates (we named it the 'Detoxifier' henceforth), which helps it possess a lower intracellular concentration of the toxic substrate (Figure 1; The second row), resulted in that the toxic substrate is less harmful to the Detoxifier than to Embezzler. Accordingly, Detoxifier is favored when the substrate is toxic.

It is important to reveal the effects of substrate concentration and toxicity on the structure of the MDOL community. To test the above two hypotheses and reveal how substrate traits shape the structure of microbial community engaged in MDOL, in this study, we combined mathematical modelling and experimentation using a synthetic microbial community. We also tested whether these effects are different when the community grows in spatially well-mixed and structured environments.

Results

Testing of our hypotheses in a well-mixed system

An ODE model for modelling the dynamics of a community engaged in MDOL

To test our hypotheses on the effects of substrate concentration and its toxicity, we built a mathematical model to simulate the dynamics of a community engaged in metabolic division of labor (MDOL) in a well-mixed system. The dimensionless form of this model is composed of 11 ordinary differential equations (ODEs; Eqn. [4] - Eqn. [13] in Methods). As summarized in Figure 2A, we considered the degradation of an organic substrate (S) into an intermediate metabolite (I), before being degraded to the final product (P). We assumed that two strains carry out this pathway via MDOL, with the first strain only executing the first step, and the second only executing the second. Initially, only S was supplied and the initial concentration was parameterized by s_0 (nondimensional). Importantly, based on our hypothesis of 'Embezzler behavior', we assumed that, P, which is synthesized by the second strain, is the sole available resource for the growth of both strains. As a result, the second strain possesses the advantage of preferentially acquiring the resource, while the first strain only obtains those growth-limiting resource that is leaked from the second strain. Therefore, the second strain behaves as an 'Embezzler'. Moreover, biotoxicity of the substrate was imposed (Supplementary Table 3;[25]) to the growth function, and the toxic strength was mediated by parameter θ. Thus, for the scenarios where substrate is assumed to be toxic, the strain executing the first step behaves as a 'Detoxifier'. Details about the model are described in Supplementary Information S1.

Analysis of the ODE model indicates initial substrate concentration affects the structure of a MDOL community.

To test our first hypothesis stating that substrate concentration affects the structure of the community, we analyzed our ODE model omitting substrate toxicity (Figure 2A). As the dimensionless model contains 11 independent parameters (Supplementary Table 4) that may affect the structure of the community, we performed a first round of numerical simulations using 885,735 parameter sets considering realistic value ranges of all the parameters (Supplementary Information S1.3; Supplementary Table 4). Our analysis showed that the Embezzler population dominated the steady-state community in all these simulations (Supplementary Figure 2; no toxic scenarios, i.e., steady-state frequencies of Detoxifier are lower than 0.5), which was in agreement with our basic assumption of product privatization. Multivariate regression analyses further suggested that six key parameters played vital roles in shaping the structure of MDOL community (Supplementary Table 4; Supplementary Figure 3A; $p < 0.01$ and the fitting coefficient values over 0.01). Notably, s_0 was second most important according to the absolute value of the fitting coefficient. s_0 positively correlated with the steady-state proportion of the Detoxifier population, suggesting that a higher initial substrate concentration favors the Detoxifier, consistent with our first hypothesis.

Through the second round of simulations (Supplementary Information S1.3), We found that when all other five key parameters were kept constant, the steady-state proportion of the Detoxifier population (DF) increased with an increase of the initial

157 substrate concentration (Figure 2B and 2C), and can be estimated by a Monod-like
158 formula using s_0 as the function argument (Figure 2C),

159 $$DF = \frac{Fd_{max} \cdot s_0}{ks + s_0} \quad [1]$$

160 Here, Fd_{max} represents the maximum proportion of the Detoxifier populations when
161 substrate is non-toxic; ks represents the half-saturation constant. Our analysis
162 indicated that the simulation results of all tested parameter sets can be accurately
163 fitted to Eqn. [1] (Figure 2D, values of Adjusted R^2 mostly over 0.95), although the
164 best fitting of Fd_{max} and ks were affected by the values of other five key parameters
165 (Figure 2E and 2F; Supplementary Information S1.3; Supplementary Table 5;
166 Supplementary Figure 4-5). Together, these results suggest that, in the absence of
167 substrate toxicity, the proportion of the Detoxifier population increases nonlinearly
168 with the increase of the initial substrate concentration, and maintains a maximum
169 value.

170 To investigate why substrate concentration governs the structure of a community, we
171 next analyzed the intracellular and extracellular concentration of final product of the
172 two populations. We found that with the increase of initial substrate concentration, the
173 fraction of final product released by the Embezzler population increased
174 (Supplementary Figure 6A-H; Supplementary Figure 6I, Red dots). As a consequence,
175 the Detoxifier obtained more product from the environment, resulting in a higher
176 intracellular product concentration, gradually approaching that of the Embezzler.
177 Moreover, based on the first hypothesis, the intracellular product concentration of the
178 Detoxifier should never exceed that of the Embezzler, even if the substrate

concentration was elevated to high levels. This prediction was confirmed by our analyses (Supplementary Figure 6A-H; Supplementary Figure 6I, blue dots). As a result, Embezzler cells still maintained their advantage from privatizing final product. This result suggests that in the absence of substrate toxicity, the benefit from product privatization obtained by the Embezzler population cannot be completely eliminated by simply increasing the substrate concentration. This observation matched with our result that the maximum proportion of the Detoxifier population (Fd_{max}) never exceeded 0.5 (Figure 2F; Supplementary Figure 5). In summary, these results suggest that substrate concentration affects the structure of the community engaged in MDOL by affecting the amount of the final product released by Embezzler (Figure 1; the first row).

Analysis of the ODE model indicates that substrate toxicity affects the structure of a MDOL community.

To test our second hypothesis, we next employed an ODE model that included the parameter of substrate toxicity (Figure 3A). Applying similar simulation and analysis method as used in the above section (Supplementary Information S1.3), we found that the toxic strength (θ) of substrate also played a significant role in structure the MDOL community. θ exhibited a significantly positive relationship with the final proportion of the Detoxifier population (Figure 3B; Supplementary Figure 2-3; Supplementary Table 4), in agreement with our second hypothesis. We then upgraded Eqn. [1] to collectively consider the effects of substrate concentration and its toxicity (Figure 3C), as follow

$$DF = \frac{Fd_{max} \cdot s_0}{ks + s_0} \cdot \left(1 + \frac{Ts_{max} \cdot \theta s_0}{kt + \theta s_0}\right) \quad [2]$$

In Eqn. [2], we use term $1 + \frac{Ts_{max} \cdot \theta s_0}{kt + \theta s_0}$ to describe the effect of substrate toxicity on the proportion of the Detoxifier populations. Ts_{max} represents the maximum fold increase of Detoxifier proportion benefiting from the substrate toxicity; ks represents the half-saturation constant of this toxic effect. This term is positively affected by the toxic strength (θ) and substrate concentration (s_0), since increasing either toxic strength or substrate concentration harms population growth (see Eqn. [12]-[13] in Methods and Supplementary Table 3). Our analyses further indicated that the *DF* values derived from numerical simulations accurately fitted to the values predicted by Eqn. [2] (Figure 3D; values of Adjusted R^2 mostly over 0.90; see Supplementary Table 5, and Supplementary Figure 7-10 for parameter sensitive analyses). These results suggest that when substrate toxicity was taken into account, the proportion of the Detoxifier population increased with both the initial concentration and the toxic strength of the substrate.

To address why substrate toxicity affects structure of the community, we next analyzed the intracellular and extracellular concentration of both S and P of the two populations. As shown in Supplementary Figure 11, the fraction of final product released by the Embezzler population largely agrees with the result derived from those non-toxic scenarios, suggesting that the presence of substrate toxicity does not change the leakiness of final product from the Embezzler. Our analysis of the S concentration showed that the Detoxifier population generally maintained a lower intracellular concentration level of S than that of the Embezzler (Supplementary

Figure 12), due to its conversion of S, thus possessing a growth advantage over the Embezzler population. Based on this mechanism, higher speed of the first reaction, or lower S transport rate, appears to favor the Detoxifier population since these two conditions assist Detoxifier in maintaining a lower intracellular S concentration. Consistent with this corollary, Ts_{max} was significantly positively correlated with a_1 and significantly negatively correlated with γ_s (Supplementary Table 5; Supplementary Figure 10). Overall, these results indicated that the difference in intracellular concentration of substrate is the main reason why substrate toxicity favors the Detoxifier population (Figure 1; second row).

When we assessed the community structure at different conditions of substrate traits, we found that Detoxifier population dominated the community when the substrate concentration and substrate toxicity were sufficiently high (its relative proportion exceeded 50% of the community; Figure 3C; Supplementary Figure 2), suggesting that the benefit from product privatization of the Embezzler can be neutralized by higher substrate concentration and toxicity. This phenomenon is quantitively characterized by Eqn. [2]: the maximum Detoxifier proportion (Fd_{max}) never exceed 0.5 in the absence of substrate toxicity (Supplementary Figure 8), but substrate toxicity can assist Detoxifier in breaking through this constraint, as quantified by the term $1+\frac{Ts_{max}\cdot\theta s_0}{kt+\theta s_0}$.

In summary, our simulations clearly showed that when a compound degradation pathway is executed through MDOL in a community, both increasing substrate concentration and toxicity of the substrate favor the Detoxifier population, resulting in

245 substrate traits to shape the structure of the community.

246 *Experimental evaluation of our rule using a liquid culture of a synthetic microbial*
247 *consortium engaged in MDOL*

248 To experimentally test the prediction from our ODE model, we engineered a synthetic
249 consortium composed of two *P. stutzeri* strains, which cooperatively degrade an
250 organic compound, salicylate, via MDOL (Figure 4A). In this synthetic consortium,
251 strain *P. stutzeri* AN0010 only retained its ability to convert toxic substrate, salicylate
252 to the intermediate catechol [33], behaving as the 'Detoxifier'; the second strain, *P.*
253 *stutzeri* AN0001, was only able to metabolize catechol, but possessed the preferential
254 access to the final product, i.e., pyruvate and acetyl-CoA (Figure 4A), the direct
255 carbon source of both strains, thus behaving as the 'Embezzler'. Details about the
256 strain construction are described in Supplementary Information S3. For simplicity, we
257 henceforth refer to our community as 'SMC-mdol'.

258 We first derived a function to predict the structure of our synthetic consortium based
259 on our model using experimentally measured or previously reported parameters
260 (Figure 4B; Supplementary Table 6; Supplementary Information S1.3). We quantified
261 the toxicity of salicylate (see Supplementary Information S3.4 for measurement
262 details), and the measured dimensionless value of toxic strength (θ) of salicylate was
263 0.0032 (Supplementary Figure 13). Accordingly, we mathematically predicted the
264 effects of substrate traits on the structure of SMC-mdol, as indicated by the red line in
265 Figure 4B and 4C. In the liquid minimal medium supplemented with different
266 concentrations of salicylate, SMC-mdol exhibited similar dynamics to that from our

corresponding ODE simulations (Supplementary Figure 14). The steady-state proportion of Detoxifier population increased from 25.6% ± 2.5% to 61.1% ± 2.6% as a function of initial salicylate concentration (Figure 4C). Moreover, our prediction function accurately estimated the steady-state structure of SMC-mdol, with a predictive power (Adjusted R^2) of 0.983. Importantly, when the substrate concentration reached high levels, the Detoxifier population dominated the community (i.e., its relative fraction over 50 %), suggesting that substrate toxicity considerably affected the structure of our consortium. Together, these experiments confirmed our simple rule proposed from mathematical modelling, and suggested that the structure of microbial community engaged in MDOL are governed by concentration and toxicity of the substrate.

Testing our hypotheses in spatially structured environments

In the above modeling and experiments, we investigated how substrate traits affect the structure of a MDOL community, principally by assuming that the substances and cells were well-mixed in the system. However, microorganisms frequently grow in spatially structured environments [34-36]. Previous studies reported that different physical characteristics between the well-mixed and spatially structured systems significantly affected the structure of a community [37-40]. Therefore, we set out to test whether our rule derived from the assumption of a well-mixed system can be expanded to estimate the structure of a MDOL community in spatially structured environments.

Individual-based modelling of the dynamics of a MDOL community.

To develop a mathematical framework to simulate the dynamics of MDOL community in spatially structured environment, we built an individual-based (IB) model. The basic configuration of our IB model was identical to the framework of our ODE model. Moreover, we assumed that the diffusion of S, I, and P was limited in the IB model, and mediated by their diffusion coefficients (D_s , D_i, and D_p). Details about the IB model are described in Supplementary Information S2.

To test our hypotheses, we ran the IB model using the parameters consistent with our experimental system (Supplementary Table 7), but varied the toxic strength (θ) and initial concentration of the substrate (s_0). We found that during the colony growth, cell lineages of Detoxifier and Embezzler segregated at frontiers, forming adjacent red and green cell sectors (Figure 5A; Supplementary video 1-4). Analysis of the spatial distribution of S, I, and P suggested that the development of this colony characteristic was mainly attributed to the 'active layer effect' reported previously [41]. As S is generally supplied from the outside of the colony, a thin active cell layer formed depending on the penetration of S, I and P (Supplementary video 1-4). Consequently, community structures in the inoculating and expanding regions may differ. Accordingly, we separately analyzed the structures in the inoculating region and expanding region of the colonies (Supplementary Figure 15). We found that with the growth of colony, community structures in the inoculating region changed little, while the community structures in the expanding region shifted over time, gradually approaching a steady-state (Supplementary Figure 16). Therefore, we next investigated how substrate traits affect the steady-state structures of the MDOL

311 community in the expanding regions. the community structure in the expanding
312 region was significantly affected by substrate traits, and can be well estimated by the
313 rule (Eqn. [2]) that we proposed for a well-mixed system (Figure 5B; Supplementary
314 Figure 17). This result indicated that the structure of the MDOL community in
315 spatially structured environments can also be estimated by the proposed simple
316 formula governed by substrate traits.
317 We also found that increasing substrate concentration assisted Detoxifier to obtain
318 more product from the environment, thus retaining higher intracellular product
319 concentrations (Supplementary Figure 18). Furthermore, Detoxifier cells possessed a
320 lower intracellular concentration level of S than that of the Embezzler cells in our IB
321 simulations (Supplementary Figure 19); higher speed of the first reaction, or lower S
322 transport rate, also significantly increased the maximum benefit (Ts_{max}) that
323 Detoxifier cells can obtained from substrate toxicity (Supplementary Figure 20;
324 correlation analysis p<0.0001), same as our results from ODE modelling. Therefore,
325 same mechanisms as in the well-mixed system are also applicable to explain why
326 substrate traits affects the structure of MDOL community in spatially structured
327 environments.
328 *Experimental evaluation of our rule by culturing our synthetic microbial consortium*
329 *in spatially structured environment.*
330 We next experimentally tested our hypotheses in spatially structured environments.
331 Several studies have reported that type IV pilus may affected the microbial colony
332 patterns [42-44]. To directly focus on the effects of substrate traits and avoid the

effects of pili, we deleted the *pilA* and *pilB* genes of the both strains involved in our synthetic consortium. This design follows other studies that performed patterning experiments using non-motile strains [45-48]. The derived consortium was named as SMC-mdolΔ*pilAB*. As shown in Fig. 4C, this strain modification did not change the effects of substrate traits on the structures of the consortium in well-mixed system, as well as the salicylate toxicity to the strains (Supplementary Figure 13).

To test our hypotheses, we cultured SMC-mdolΔ*pilAB* on an agarose surface to which salicylate was added at different concentrations. The experimentally observed colony patterns were very similar to those observed in the simulations (Figure 5C). We next separately assessed the structures of the consortium in both the inoculating region and expanding region of the colonies. We found that the proportion of Detoxifier population slightly shifted from 40.9% ± 3.5% to 60.0% ± 6.0% in the inoculating region (Supplementary Figure 21), but it largely varied from 17.4% ± 1.5% to 69.0% ± 7.0% in the expanding region (Figure 5D). Importantly, the experimental results of expanding region accurately fitted to our derived prediction function (Figure 5D) with a predicting power (Adjusted R^2) of 0.982. Together, our simulations and experiments demonstrated that our rules on how substrate traits shape the structure of MDOL community were applicable when this community grew in a spatially structured environment.

The effects of substance diffusivity on the structure of the MDOL community

Although the structure of MDOL community in spatially structured and well-mixed environments can both be estimated by Eqn. [2], the estimated parameter values in the

355 prediction functions derived from ODE and IB model are slightly different (Figure 4
356 and 5), even if we applied identical parameters and equations in these two models
357 (Supplementary Information S2.3). Through mathematical modelling, we revealed
358 that limited mass diffusion is one of the major reasons that lead to this difference (see
359 Supplementary Information 2.2 for detail). Our analyses suggested that higher level of
360 P diffusion favors the Detoxifier (Supplementary Figure 22-23), whereas increasing
361 the diffusion level of I harms the Detoxifier (Supplementary Figure 24-25).
362 In addition, we found that the diffusion level of substrate has two opposing effects on
363 the structure of MDOL community. On the one hand, higher diffusion level of S
364 benefits Detoxifier (Figure 6A, first row), through thickening the cell's 'active layer'
365 (Figure 6B; [48]), and thus increasing production and secretion of the final product by
366 Embezzler cells. On the other hand, higher diffusion level of S also decreases the
367 fitness of the Detoxifier cells by modifying the concentration gradient of S around the
368 two types of cells, and thus changing relative toxic level of S (Figure 6A, second row;
369 Supplementary Figure 26). Combining these two effects, we formulated a new
370 formula to estimate the structure of MDOL community

371 $$DF = \frac{Fd_{max} s_0}{ks+s_0} \cdot (1 + \frac{Ts_{max} \theta s_0}{kt+\theta s_0}) \cdot (\frac{s_0 D_s}{kd_1+s_0 D_s} - \frac{\theta D_s}{kd_2+\theta D_s}) \quad [3]$$

372 In this formula, $\frac{s_0 D_s}{kd_1+s_0 D_s}$ represents an estimate of the positive effect of increasing
373 substrate diffusion level via thickening cell 'active layer', related to the initial
374 substrate concentration (s_0; Figure 6B; [48]); $\frac{\theta D_s}{kd_2+\theta D_s}$ represents an estimate of the
375 negative effect of increasing substrate diffusion level, influenced by toxic strength of
376 the substrate (Figure 6A; the second row). Eqn. [3] accurately estimated the structure

377 of MDOL community in our IB simulations (Figure 6C; R^2=0.994). Overall, we
378 concluded that the traits of substrate, including concentration, toxicity, and diffusivity,
379 are fundamental to shaping the structure of MDOL community.
380

Discussion

Here we show how substrate traits shape the structure of the microbial communities engaged in metabolic division of labor (MDOL) when degrading organic compounds. The population performing the first step is favored by both higher substrate concentration and its toxicity. This rule is applicable when the community grow both in a well-mixed and a spatially structured environment.

Recently, numerous studies have explored the strategy of dividing metabolic roles across different populations in a consortium toward removal of organic pollutants [8, 49-53]. Our proposed rule may be expanded to forecast the structure of these consortia. For instance, one recent study reported that a bacterial consortium composed of *Leucobacter* sp. GP and *Achromobacter denitrificans* PR1 efficiently degrades an antibiotic, sulfamethoxazole, in which the strain GP is responsible for the initial metabolism of the sulfamethoxazole (Detoxifier), and the strain PR1 carries out the subsequent conversion (Embezzler)[12]. This study measured the structures of the community across a gradient of initial substrate concentrations, and found that the proportion of the GP is positively correlated with the initial sulfamethoxazole concentration. This observation largely agrees with the idea derived from our model and experiments. The prediction on the structure of community may largely help to manage these communities for better performance [15, 28, 29].

Our study also indicated that limited mass diffusion in spatially structured environments is one key factor to determine the structure of a community. This finding is reminiscent of recent studies proposing that limited mass diffusion plays

403 significant role on the structure of the communities engaged in other diffusion-based
404 interaction modes, including syntrophic exchange [37, 40, 54], cross-protection [55],
405 and 'rock-paper-scissors' interaction [56, 57]. One important hypothesis from these
406 studies is that limited mass diffusion is one possible way to privatize public benefit
407 [37, 40, 58]. We found this hypothesis is also applicable to explain the structuring of
408 the community engaged in MDOL. On the one hand, limited mass diffusion helps the
409 Embezzler population to privatize the final product for its own growth. On the other
410 hand, it helps the Detoxifier population to privatize its benefit from detoxification.
411 Therefore, limited mass diffusion may be a universally used avenue for
412 microorganisms to maintain their private benefit in spatially structured environments.
413 In our IB modelling, we also found that specific spatial patterns developed by the
414 MDOL community. In agreement with previous studies [39, 59, 60], when two
415 populations engaged in MDOL, cells from the two populations are spatially more
416 proximal to each other than the scenario when the two populations did not exhibit
417 defined interactions (Supplementary Figure 27). In addition, we also found that the
418 level of spatial proximity was governed by substrate traits (Supplementary Figure 27).
419 Interestingly, when the strength of substrate toxicity was higher, the Detoxifier cells
420 occupied the periphery of the growing colony, forming a clearly 'ring' around the
421 colony (Figure 5; Supplementary video 3; Supplementary Figure 28). The formation
422 of this ring might be due to the fact that the substrate was present at higher
423 concentrations at the colony edge, and hence more toxic, thus largely favoring
424 Detoxifier cells at edge. These results suggest that substrate traits also govern the

425 spatial distributions of different cells in the colony developed by MDOL community,
426 which may in turn, affect the structure of such community. Although we did not
427 observe this featured cell distribution in our experiments, one recent study found that
428 a MDOL community that degrades toluene developed a similar 'ring'-shape pattern as
429 observed in our IB model [59]. Therefore, such cell distribution may represent a
430 critical feature of the spatial patterns developed by a MDOL community that degrades
431 toxic substrates.

432 While our study provides critical new insights into how the community engaged in
433 MDOL assembles, a number of limitations need to be taken into consideration. First,
434 our model analysis showed that substrate toxicity is vital to determine the structure of
435 communities engaged in MDOL. However, due to the difficulties in manipulating the
436 toxicity of the substrate (salicylate) *in vitro*, we were unable to experimentally
437 compare the impact of the different toxic strengths on the structure of our community.
438 Nevertheless, our model correctly predicts that simply increasing the initial substrate
439 concentration is unlikely to shape a community dominated by the Detoxifier
440 population, while the presence of substrate toxicity renders the 'Detoxifier' population
441 in the community to become dominant. Therefore, the observation that Detoxifier
442 population was able to dominate the synthetic consortium when supplying high
443 concentration of salicylate, and the measured biotoxicity of salicylate strongly
444 suggested that substrate toxicity should affect the structure of our synthetic microbial
445 consortium. In agreement with this idea, our prediction functions involved in
446 salicylate toxic strength fits the experiment results very well. To further examine this

447 idea, it is necessary to design a better system in which the toxicity of the substrate can
448 be modulated.

449 Second, our ODE model suggests that apart from substrate traits, five other key
450 parameters exist that exhibit considerable effects on the structure of a MDOL
451 community. Here, we primarily focused on the effects of substrate traits, without
452 analyzing in detail how all the seven key factors collectively determine the structure
453 of community. Nonetheless, our analysis presented here suggests that biotic factors
454 such as speed of the first reaction (a_1), mass transport rate (γ_s, γ_i, γ_p), as well as
455 consumption rate of P (Cp), affected the structure of the community, namely by
456 determining the value of parameters in Eqn. [2] (i.e., Fd_{max}, ks, Ts_{max}, and kt).
457 However, due to the difficulties in analytically solving non-linear ODEs, as well as
458 the low efficiency of individual-based simulations [61], detailed quantitative
459 understanding of how all these factors affect the structure of MDOL community
460 remains limited. Further studies may use more simplified models that combine these
461 elements to provide a more general description of the principles governing the
462 structuring of a MDOL community.

463 To engineer stable and high-efficient microbial systems for bioproduction or
464 biodegradation, it will be critical to predict how the communities assembled by a
465 given set of strains exhibiting modularized functions. Our results demonstrate that, for
466 a given community engaged in MDOL, its structure can be quantitatively estimated
467 from the abiotic factors, such as the traits of its substrate, suggesting that it is feasible
468 to manage microbial communities through manipulation of specific environmental

469 factors, to address grand challenges facing human society in agriculture, degradation

470 of the environment, and human health.

471

Methods

Formulation and analyses of the ODE model

Formulation of the ODE model

To simulate the dynamics of a MDOL community in well-mixed system, a mathematical model was formulated using ordinary differential equations (ODEs). Here, the dimensionless forms of the models were presented. The detailed derivations of the models, and choices of parameter values are described in Supplementary Information S1.

As described in the Results section, a two-step pathway was assumed to be implemented by MDOL between two populations (Figure 2A and Figure 3A). For simplicity, the basic model was built based on five simple assumptions: (1) The systems are well mixed in each compartment (inside a cell or in the extracellular space). (2) transport of substrate (S), intermediate (I) and final product (P) is mediated by passive diffusion; (3) P was assumed to be the sole and limited resource for the growth of the two populations and its consumption was calculated following Monod equations; (4) Basic biological properties (the coefficients in Monod equations) regarding the growth of the two populations are identical, since we only focused on the effects of abiotic factors; (5) when applicable, substrate toxicity was introduced by adding three different toxic terms to the growth equation (Supplementary Table 3), dependent on intracellular S concentration of the corresponding population. The dynamics of intracellular and extracellular I and P are given by

$$\frac{ds_{1,in}}{d\tau} = -\frac{a_1}{1+s_{1,in}} s_{1,in} + \gamma_s \cdot \left(s_{out} - s_{1,in}\right) \quad [4]$$

494 $$\frac{ds_{2,in}}{d\tau} = \gamma_s \cdot \left(s_{out} - s_{2,in}\right) \quad [5]$$

495 $$\frac{di_{1,in}}{d\tau} = \frac{a_1}{1+s_{1,in}} s_{1,in} - \gamma_i \cdot \left(i_{1,in} - i_{out}\right) \quad [6]$$

496 $$\frac{di_{2,in}}{d\tau} = -\frac{a_2}{\beta_2 + i_{2,in}} i_{2,in} + \gamma_i \cdot \left(i_{out} - i_{2,in}\right) \quad [7]$$

497 $$\frac{dp_{1,in}}{d\tau} = -\frac{Cp}{\beta_g + p_{1,in}} p_{1,in} + \gamma_p \cdot \left(p_{out} - p_{1,in}\right) \quad [8]$$

498 $$\frac{dp_{2,in}}{d\tau} = \frac{a_2}{\beta_2 + i_{2,in}} i_{2,in} - \frac{Cp}{\beta_g + p_{2,in}} p_{2,in} + \gamma_p \cdot \left(p_{out} - p_{2,in}\right) \quad [9]$$

499 $$\frac{ds_{out}}{d\tau} = -x_1 \cdot \gamma_s \cdot \left(s_{out} - s_{1,in}\right) - x_2 \cdot \gamma_s \cdot \left(s_{out} - s_{2,in}\right) \quad [10]$$

500 $$\frac{di_{out}}{d\tau} = x_1 \cdot \gamma_i \cdot \left(i_{out} - i_{1,in}\right) - x_2 \cdot \gamma_i \cdot \left(i_{out} - i_{2,in}\right) \quad [11]$$

501 $$\frac{dp_{out}}{d\tau} = x_2 \cdot \gamma_p \cdot \left(p_{out} - p_{1,in}\right) - x_1 \cdot \gamma_p \cdot \left(p_{out} - p_{1,in}\right) \quad [12]$$

502 The growth of the two populations was modeled using a general logistic function with

503 first-order cell death:

504 $$\frac{dx_1}{d\tau} = \frac{Cp}{bg + p_{1,in}} p_{1,in} yt_1 x_1 \left(1 - \frac{x_1 + x_2}{\rho}\right) \quad [13]$$

505 $$\frac{dx_2}{d\tau} = \frac{Cp}{bg + p_{2,in}} p_{2,in} yt_2 x_2 \left(1 - \frac{x_1 + x_2}{\rho}\right) \quad [14]$$

506 The definitions and dimensionless methods of all variables are listed in

507 Supplementary Table 1. The definitions and dimensionless methods, as well as the

508 value ranges of all the parameters involved in these equations are listed in

509 Supplementary Table 2.

510 *Simulation and analyzing protocol of the ODE model*

511 Details of the simulation and analysis protocols of our ODE model and the

512 downstream analyses are described in Supplementary Information S1.3. Briefly, to

513 solve the community dynamics of the MDOL community with given parameter sets,

514 numerical simulations of our ODE model were performed using *NDsolve* function of

515 *Wolfram Mathematica*. The numerical solutions of all the variables, including the

dynamics of mass (S, I, P) concentration and biomass, were recorded for further analyses. To perform simulations with numerous parameter sets, as well as the downstream analysis, custom *Mathematica* scripts were wrote mainly based on the *Do* loop function.

Individual-based modeling

Our individual based (IB) model was constructed based on *gro* platform (https: https://github.com/liaupm/GRO-LIA), a simulator designed by Gutiérrez and colleagues aiming to describe multicellular bacterial behavior [62]. The model aims to simulate the growth of a microbial colony composed of two populations who execute substrate degradation via MDOL on a surface. The model was formulated mainly using the same equations as our dimensional ODE model (Supplementary Information S1.1, Eqns. [S1]-[S13]) to characterize the intra- and extracellular dynamics of mass (S, I, P) concentration, as well as to calculate the rate of cell growth. Four main differences exist between our IB model and the ODE model: (1) The IB model was formulated on a spatially structured surface, and the diffusion of S, I, and P was limited; (2) Mass dynamics was modelled at single-cell level; (3) The growth of both populations was modelled at single-cell level, and passive cell shoving during the cell growth was included; (4) cells were inoculated in the center of the surface, and the entire community underwent 'colony range expansion', a process whereby the community immigrate outwards as a whole, driven by the force generated from cell growth and division (Supplementary Figure 15). The mathematical framework formulating these four points is described in Supplementary Information S2.1. To

implement our design of the IB model, custom codes were written in *gro* language. Variables and Parameters in the IB model are summarized in Supplementary Table 7. Details of the IB simulation workflow are described in Supplementary Information S2.

Experimental verification of our model prediction

Genetic manipulation of the P. stutzeri strains

All *P. stutzeri* strains were engineered from a naphthalene-degrading bacterial strain *P. stutzeri* AN10 [63]. Genes that encode the key enzymes responsible for corresponding metabolic steps in salicylate degradation pathway were knocked out to generate the *P. stutzeri* strains. The details of the genetic manipulation of are described in Supplementary information S3.

Liquid cultivation of our synthetic microbial communities

Liquid cultivation of our synthetic microbial communities was performed in 96-well plates that contains 120 μL fresh minimum medium. Proportions of the two populations in the community were estimated by measuring the fluorescent intensity of the two strains involved using a microplate reader (Molecular Devices, Sunnyvale, America). Detailed protocols are described in Supplementary information S4.

Colony pattern formation assays

Colony pattern formation assays were performed on the agarose surface in a Petri dish (60 mm in diameter). Images of the colony patterns were taken under a 5× objective using a Leica DM6000B fluorescence microscope (Leica Corporation, Wetzlar, Germany) equipped with a LED fluorescence illuminator (Leica Corporation). The

relative fraction of each population in the colonies was measured by image analysis, as well as similar fluorescence-measurement method as performed in liquid cultivation experiments. Detailed protocols are described in Supplementary information S5.

Statistical analysis

Unless indicated otherwise, the number of replicates was three for each simulation, and six for each experiment. For comparative statistics, unpaired, two-tailed, Student's t-test was performed in Wolfram Mathematica (version 12.4). To fit the data to the proposed function, Nonlinearmodelfit function of the Wolfram Mathematica (version 12.4) was applied.

Code availability

All custom *Mathematica* codes used for ODE simulation and data analyses, as well as the source *gro* codes used for our IB simulations are available at Github: https://github.com/RoyWang1991/MDOLcode/tree/master/MDOL-spatial.

Competing Interests

The authors declare that they have no conflict of interest.

Acknowledgments

We wish to thank Professor Ping Xu (Shanghai Jiao Tong University, Shanghai, P.R. China) for supplying plasmid pMMPc-Gm, used for fluorescence labeling in this study; Dr. Min Lin (Chinese Academy of Agricultural Sciences, Beijing, P.R. China) for providing plasmid pK18mobsacB and pRK2013, used for genetic engineering in this work; Professor Martin Ackermann (ETH Zurich, Zurich, Switzerland), Dr. David

582 Johnson (Eawag, Dübendorf, Switzerland) and Yinyin Ma (Eawag, Dübendorf,
583 Switzerland) for constructive inputs on the design of this study; Professor Martín
584 Gutiérrez (Universidad Politécnica de Madrid, Madrid, Spain) for his kindly guidance
585 for the set-up of the *gro* platform for the individual-based simulations; Dr. T. Juelich
586 (UCAS, Beijing) for linguistic assistance during the preparation of this manuscript.
587 This work was supported by National Key R&D Program of China
588 (2018YFA0902100 and 2018YFA0902103), and National Natural Science Foundation
589 of China (91951204, 31761133006, 31770120, and 31770118).
590

References

1. Kreft JU, Griffin BM, Gonzalez-Cabaleiro R. Evolutionary causes and consequences of metabolic division of labour: why anaerobes do and aerobes don't. Curr Opin Biotechnol. 2020;62:80-7; doi:10.1016/j.copbio.2019.08.008.

2. Tsoi R, Wu F, Zhang C, Bewick S, Karig D, You L. Metabolic division of labor in microbial systems. Proc Natl Acad Sci U S A. 2018;115:10:2526-31; doi:10.1073/pnas.1716888115.

3. Harvey E, Heys J, Gedeon T. Quantifying the effects of the division of labor in metabolic pathways. J Theor Biol. 2014;360:222-42; doi:10.1016/j.jtbi.2014.07.011.

4. Thommes M, Wang T, Zhao Q, Paschalidis IC, Segre D. Designing Metabolic Division of Labor in Microbial Communities. mSystems. 2019;4:2; doi:10.1128/mSystems.00263-18.

5. Schink B, Pfennig N. Fermentation of Trihydroxybenzenes by Pelobacter-Acidigallici Gen-Nov Sp-Nov a New Strictly Anaerobic, Non-Sporeforming Bacterium. Arch Microbiol. 1982;133:3:195-201; doi:Doi 10.1007/Bf00415000.

6. Wang CY, Huang Y, Zhang ZT, Hao H, Wang H. Absence of the nahG-like gene caused the syntrophic interaction between *Marinobacter* and other microbes in PAH-degrading process. J Hazard Mater. 2020;384; doi:ARTN 12138710.1016/j.jhazmat.2019.121387.

7. Katsuyama C, Nakaoka S, Takeuchi Y, Tago K, Hayatsu M, Kato K. Complementary cooperation between two syntrophic bacteria in pesticide degradation. Journal of Theoretical Biology. 2009;256:4:644-54; doi:10.1016/j.jtbi.2008.10.024.

8. Yang C, Li Y, Zhang K, Wang X, Ma C, Tang H, Xu P. Atrazine degradation by a simple consortium of *Klebsiella* sp. A1 and *Comamonas* sp. A2 in nitrogen enriched medium. Biodegradation. 2010;21:1:97-105; doi:10.1007/s10532-009-9284-9.

9. Billet L, Devers M, Rouard N, Martin-Laurent F, Spor A. Labour sharing promotes coexistence in atrazine degrading bacterial communities. Sci Rep. 2019;9:1:18363; doi:10.1038/s41598-019-54978-2.

620 10. Gilbert ES, Walker AW, Keasling JD. A constructed microbial consortium for
621 biodegradation of the organophosphorus insecticide parathion. Appl Microbiol Biot.
622 2003;61:1:77-81; doi:10.1007/s00253-002-1203-5.
623 11. Meyer-Cifuentes IE, Werner J, Jehmlich N, Will SE, Neumann-Schaal M, Ozturk
624 B. Synergistic biodegradation of aromatic-aliphatic copolyester plastic by a marine
625 microbial consortium. Nature Communications. 2020;11:1; doi:ARTN
626 579010.1038/s41467-020-19583-2.
627 12. Reis AC, Cvancarova M, Liu Y, Lenz M, Hettich T, Kolvenbach BA, Corvini PFX,
628 Nunes OC. Biodegradation of sulfamethoxazole by a bacterial consortium of
629 *Achromobacter denitrificans* PR1 and *Leucobacter* sp GP. Appl Microbiol Biot.
630 2018;102:23:10299-314; doi:10.1007/s00253-018-9411-9.
631 13. Zheng H, Perreau J, Powell JE, Han BF, Zhang ZJ, Kwong WK, Tringe SG,
632 Moran NA. Division of labor in honey bee gut microbiota for plant polysaccharide
633 digestion. P Natl Acad Sci USA. 2019;116:51:25909-16;
634 doi:10.1073/pnas.1916224116.
635 14. Peng XF, Wilken S, Lankiewicz TS, Gilmore SP, Brown JL, Henske JK, Swift CL,
636 Salamov A, Barry K, Grigoriev IV, Theodorou MK, Valentine DL, O'Malley MA.
637 Genomic and functional analyses of fungal and bacterial consortia that enable
638 lignocellulose breakdown in goat gut microbiomes. Nat Microbiol. 2021;6:4:499-+;
639 doi:10.1038/s41564-020-00861-0.
640 15. Cao X, Hamilton JJ, Venturelli OS. Understanding and Engineering Distributed
641 Biochemical Pathways in Microbial Communities. Biochemistry-Us.
642 2019;58:2:94-107; doi:10.1021/acs.biochem.8b01006.
643 16. Koudryashova Y, Chizhova T, Tishchenko P, Hayakawa K. Seasonal Variability of
644 Polycyclic Aromatic Hydrocarbons (PAHs) in a Coastal Marine Area in the
645 Northwestern Region of the Sea of Japan/East Sea (Possiet Bay). Ocean Sci J.
646 2019;54:4:635-55; doi:10.1007/s12601-019-0031-9.
647 17. Jiang Y, Hu X, Yves UJ, Zhan H, Wu Y. Status, source and health risk assessment
648 of polycyclic aromatic hydrocarbons in street dust of an industrial city, NW China.
649 Ecotoxicol Environ Saf. 2014;106:11-8; doi:10.1016/j.ecoenv.2014.04.031.

18. Ozaki N, Takamura Y, Kojima K, Kindaichi T. Loading and removal of PAHs in a wastewater treatment plant in a separated sewer system. Water Res. 2015;80:337-45; doi:10.1016/j.watres.2015.05.002.

19. Boethling RS, Alexander M. Effect of Concentration of Organic-Chemicals on Their Biodegradation by Natural Microbial Communities. Appl Environ Microb. 1979;37:6:1211-6; doi:Doi 10.1128/Aem.37.6.1211-1216.1979.

20. Fernandez J, Perez M, Romero LI. Effect of substrate concentration on dry mesophilic anaerobic digestion of organic fraction of municipal solid waste (OFMSW). Bioresource Technol. 2008;99:14:6075-80; doi:10.1016/j.biortech.2007.12.048.

21. Zhao J, Westerholm M, Qiao W, Yin DM, Bi SJ, Jiang MM, Dong RJ. Impact of temperature and substrate concentration on degradation rates of acetate, propionate and hydrogen and their links to microbial community structure. Bioresource Technol. 2018;256:44-52; doi:10.1016/j.biortech.2018.01.150.

22. Monod J. The Growth of Bacterial Cultures. Annual Review of Microbiology. 1949;3:371-94; doi:DOI 10.1146/annurev.mi.03.100149.002103.

23. Peng RH, Xiong AS, Xue Y, Fu XY, Gao F, Zhao W, Tian YS, Yao QH. Microbial biodegradation of polyaromatic hydrocarbons. Fems Microbiol Rev. 2008;32:6:927-55; doi:10.1111/j.1574-6976.2008.00127.x.

24. Park W, Jeon CO, Cadillo H, DeRito C, Madsen EL. Survival of naphthalene-degrading *Pseudomonas putida* NCIB 9816-4 in naphthalene-amended soils: toxicity of naphthalene and its metabolites. Appl Microbiol Biot. 2004;64:3:429-35; doi:10.1007/s00253-003-1420-6.

25. Quintas C, Leyva JS, Sotoca R, Loureiro-Dias MC, Peinado JM. A model of the specific growth rate inhibition by weak acids in yeasts based on energy requirements. Int J Food Microbiol. 2005;100:1-3:125-30; doi:10.1016/j.ijfoodmicro.2004.10.009.

26. Pumphrey GM, Madsen EL. Naphthalene metabolism and growth inhibition by naphthalene in *Polaromonas naphthalenivorans* strain CJ2. Microbiology (Reading). 2007;153:Pt 11:3730-8; doi:10.1099/mic.0.2007/010728-0.

27. Joesaar M, Viggor S, Heinaru E, Naanuri E, Mehike M, Leito I, Heinaru A.

Strategy of *Pseudomonas pseudoalcaligenes* C70 for effective degradation of phenol and salicylate. PLoS One. 2017;12:3:e0173180; doi:10.1371/journal.pone.0173180.

28. Graham EB, Knelman JE, Schindlbacher A, Siciliano S, Breulmann M, Yannarell A, Bemans JM, Abell G, Philippot L, Prosser J, Foulquier A, Yuste JC, Glanville HC, Jones DL, Angel F, Salminen J, Newton RJ, Burgmann H, Ingram LJ, Hamer U, Siljanen HMP, Peltoniemi K, Potthast K, Baneras L, Hartmann M, Banerjee S, Yu RQ, Nogaro G, Richter A, Koranda M, Castle SC, Goberna M, Song B, Chatterjee A, Nunes OC, Lopes AR, Cao YP, Kaisermann A, Hallin S, Strickland MS, Garcia-Pausas J, Barba J, Kang H, Isobe K, Papaspyrou S, Pastorelli R, Lagomarsino A, Lindstrom ES, Basiliko N, Nemergut DR. Microbes as Engines of Ecosystem Function: When Does Community Structure Enhance Predictions of Ecosystem Processes? Frontiers in Microbiology. 2016;7; doi:ARTN 21410.3389/fmicb.2016.00214.

29. Fuhrman JA. Microbial community structure and its functional implications. Nature. 2009;459:7244:193-9; doi:10.1038/nature08058.

30. Kato S, Haruta S, Cui ZJ, Ishii M, Igarashi Y. Stable coexistence of five bacterial strains as a cellulose-degrading community. Appl Environ Microb. 2005;71:11:7099-106; doi:10.1128/Aem.71.11.7099-7106.2005.

31. Heinrich R, Schuster S. The regulation of cellular systems. Springer Science & Business Media; 2012.

32. Wegner A, Meiser J, Weindl D, Hiller K. How metabolites modulate metabolic flux. Curr Opin Biotech. 2015;34:16-22; doi:10.1016/j.copbio.2014.11.008.

33. Lanfranconi MP, Christie-Oleza JA, Martin-Cardona C, Suarez-Suarez LY, Lalucat J, Nogales B, Bosch R. Physiological role of NahW, the additional salicylate hydroxylase found in *Pseudomonas stutzeri* AN10. Fems Microbiol Lett. 2009;300:2:265-72; doi:10.1111/j.1574-6968.2009.01787.x.

34. Nadell CD, Drescher K, Foster KR. Spatial structure, cooperation and competition in biofilms. Nat Rev Microbiol. 2016;14:9:589-600; doi:10.1038/nrmicro.2016.84.

35. Mitri S, Xavier JB, Foster KR. Social evolution in multispecies biofilms. P Natl Acad Sci USA. 2011;108:10839-46; doi:10.1073/pnas.1100292108.

710 36. Xavier JB, Foster KR. Cooperation and conflict in microbial biofilms. P Natl Acad
711 Sci USA. 2007;104:3:876-81; doi:10.1073/pnas.0607651104.
712 37. Pande S, Kaftan F, Lang S, Svatos A, Germerodt S, Kost C. Privatization of
713 cooperative benefits stabilizes mutualistic cross-feeding interactions in spatially
714 structured environments. ISME J. 2016;10:6:1413-23; doi:10.1038/ismej.2015.212.
715 38. Nadell CD, Drescher K, Foster KR. Spatial structure, cooperation and competition
716 in biofilms. Nat Rev Microbiol. 2016;14:9:589-600; doi:10.1038/nrmicro.2016.84.
717 39. Goldschmidt F, Regoes RR, Johnson DR. Successive range expansion promotes
718 diversity and accelerates evolution in spatially structured microbial populations. Isme
719 Journal. 2017;11:9:2112-23; doi:10.1038/ismej.2017.76.
720 40. Momeni B, Waite AJ, Shou W. Spatial self-organization favors heterotypic
721 cooperation over cheating. Elife. 2013;2:e00960; doi:10.7554/eLife.00960.
722 41. Nadell CD, Foster KR, Xavier JB. Emergence of Spatial Structure in Cell Groups
723 and the Evolution of Cooperation. Plos Computational Biology. 2010;6:3; doi:ARTN
724 e100071610.1371/journal.pcbi.1000716.
725 42. Klausen M, Heydorn A, Ragas P, Lambertsen L, Aaes-Jorgensen A, Molin S,
726 Tolker-Nielsen T. Biofilm formation by *Pseudomonas aeruginosa* wild type, flagella
727 and type IV pili mutants. Mol Microbiol. 2003;48:6:1511-24;
728 doi:10.1046/j.1365-2958.2003.03525.x.
729 43. Barken KB, Pamp SJ, Yang L, Gjermansen M, Bertrand JJ, Klausen M, Givskov
730 M, Whitchurch CB, Engel JN, Tolker-Nielsen T. Roles of type IV pili,
731 flagellum-mediated motility and extracellular DNA in the formation of mature
732 multicellular structures in *Pseudomonas aeruginosa* biofilms. Environ Microbiol.
733 2008;10:9:2331-43; doi:10.1111/j.1462-2920.2008.01658.x.
734 44. O'Toole GA, Kolter R. Flagellar and twitching motility are necessary for
735 *Pseudomonas aeruginosa* biofilm development. Mol Microbiol. 1998;30:2:295-304;
736 doi:10.1046/j.1365-2958.1998.01062.x.
737 45. Hallatschek O, Hersen P, Ramanathan S, Nelson DR. Genetic drift at expanding
738 frontiers promotes gene segregation. P Natl Acad Sci USA. 2007;104:50:19926-30;
739 doi:10.1073/pnas.0710150104.

740 46. Hallatschek O, Nelson DR. Life at the Front of an Expanding Population.
741 Evolution. 2010;64:1:193-206; doi:10.1111/j.1558-5646.2009.00809.x.
742 47. Korolev KS, Xavier JB, Nelson DR, Foster KR. A Quantitative Test of Population
743 Genetics Using Spatiogenetic Patterns in Bacterial Colonies. American Naturalist.
744 2011;178:4:538-52; doi:10.1086/661897.
745 48. Mitri S, Clarke E, Foster KR. Resource limitation drives spatial organization in
746 microbial groups. Isme Journal. 2016;10:6:1471-82; doi:10.1038/ismej.2015.208.
747 49. Li Z, Yoshida N, Wang A, Nan J, Liang B, Zhang C, Zhang D, Suzuki D, Zhou X,
748 Xiao Z, Katayama A. Anaerobic mineralization of 2,4,6-tribromophenol to CO2 by a
749 synthetic microbial community comprising *Clostridium*, *Dehalobacter*, and
750 *Desulfatiglans*. Bioresour Technol. 2015;176:225-32;
751 doi:10.1016/j.biortech.2014.10.097.
752 50. Che S, Men Y. Synthetic microbial consortia for biosynthesis and biodegradation:
753 promises and challenges. J Ind Microbiol Biotechnol. 2019;46:9-10:1343-58;
754 doi:10.1007/s10295-019-02211-4.
755 51. Hudcova T, Halecky M, Kozliak E, Stiborova M, Paca J. Aerobic degradation of
756 2,4-dinitrotoluene by individual bacterial strains and defined mixed population in
757 submerged cultures. J Hazard Mater. 2011;192:2:605-13;
758 doi:10.1016/j.jhazmat.2011.05.061.
759 52. Roell GW, Zha J, Carr RR, Koffas MA, Fong SS, Tang YJ. Engineering microbial
760 consortia by division of labor. Microb Cell Fact. 2019;18:1:35;
761 doi:10.1186/s12934-019-1083-3.
762 53. Jia XQ, He Y, Jiang DW, Liu C, Lu WY. Construction and analysis of an
763 engineered *Escherichia coli-Pseudomonas aeruginosa* co-culture consortium for
764 phenanthrene bioremoval. Biochem Eng J. 2019;148:214-23;
765 doi:10.1016/j.bej.2019.05.010.
766 54. Momeni B, Brileya KA, Fields MW, Shou WY. Strong inter-population
767 cooperation leads to partner intermixing in microbial communities. Elife. 2013;2;
768 doi:ARTN e0023010.7554/eLife.00230.
769 55. Frost I, Smith WPJ, Mitri S, Millan AS, Davit Y, Osborne JM, Pitt-Francis JM,

MacLean RC, Foster KR. Cooperation, competition and antibiotic resistance in bacterial colonies. ISME J. 2018;12:6:1582-93; doi:10.1038/s41396-018-0090-4.

56. Kerr B, Riley MA, Feldman MW, Bohannan BJ. Local dispersal promotes biodiversity in a real-life game of rock-paper-scissors. Nature. 2002;418:6894:171-4; doi:10.1038/nature00823.

57. Nahum JR, Harding BN, Kerr B. Evolution of restraint in a structured rock-paper-scissors community. P Natl Acad Sci USA. 2011;108:10831-8; doi:10.1073/pnas.1100296108.

58. Wang M, Liu X, Nie Y, Wu XL. Selfishness driving reductive evolution shapes interdependent patterns in spatially structured microbial communities. ISME J. 2021;15:5:1387-401; doi:10.1038/s41396-020-00858-x.

59. Tecon R, Or D. Cooperation in carbon source degradation shapes spatial self-organization of microbial consortia on hydrated surfaces. Sci Rep-Uk. 2017;7; doi:ARTN 4372610.1038/srep43726.

60. Goldschmidt F, Regoes RR, Johnson DR. Metabolite toxicity slows local diversity loss during expansion of a microbial cross-feeding community. Isme Journal. 2018;12:1:136-44; doi:10.1038/ismej.2017.147.

61. Hellweger FL, Clegg RJ, Clark JR, Plugge CM, Kreft JU. Advancing microbial sciences by individual-based modelling. Nat Rev Microbiol. 2016;14:7:461-71; doi:10.1038/nrmicro.2016.62.

62. Gutierrez M, Gregorio-Godoy P, Perez Del Pulgar G, Munoz LE, Saez S, Rodriguez-Paton A. A New Improved and Extended Version of the Multicell Bacterial Simulator gro. ACS Synth Biol. 2017;6:8:1496-508; doi:10.1021/acssynbio.7b00003.

63. Brunet-Galmes I, Busquets A, Pena A, Gomila M, Nogales B, Garcia-Valdes E, Lalucat J, Bennasar A, Bosch R. Complete Genome Sequence of the Naphthalene-Degrading Bacterium *Pseudomonas stutzeri* AN10 (CCUG 29243). J Bacteriol. 2012;194:23:6642-3; doi:10.1128/Jb.01753-12.

Figures

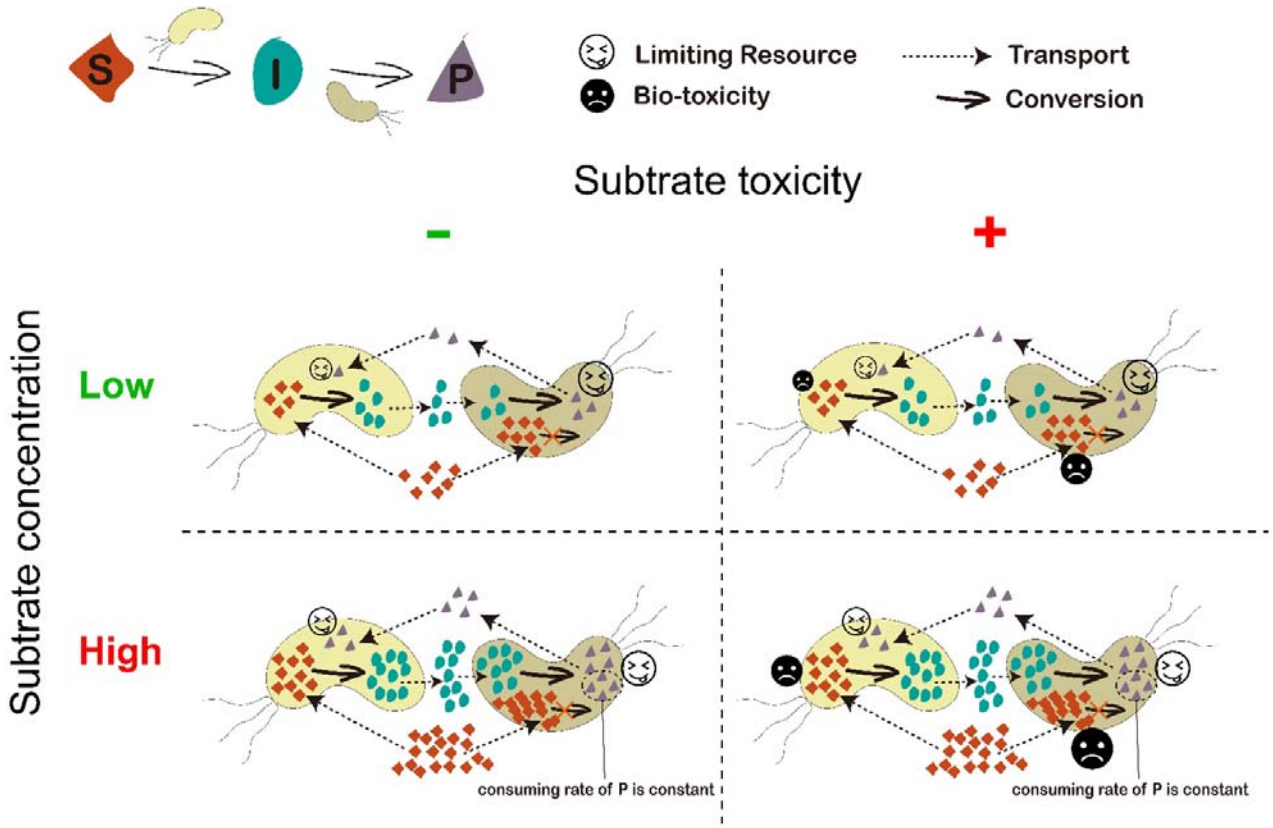

Figure 1 Hypothesis for how substrate concentration and toxicity govern the structure of community engaged in MDOL. In a community

degrading an organic compound through metabolic division of labor (MDOL), final product was assumed to be the sole resource and was synthesized by the strain performing the second step. Therefore, this strain will obtain more nutrients (denoted as bigger 'smiling face'), while the other strain has to collect product released from this population (denoted as smaller 'smiling face'). Thus, the last population was named 'Embezzler'. However, increasing the concentration of the substrate (vertical axis) improves the flux of the pathway. Since the P consuming ability of Embezzler cells is limited (dashed box), increasing the concentration will lead to higher final product leakiness, favoring the growth of the first population. Moreover, introducing substrate biotoxicity (horizontal axis) also favors the first population, because it converts this toxic substrate (denoted as smaller sad face), resulting in lower intracellular substrate concentration compared to that of the Embezzler cells (denoted as bigger sad face). Thus, the first population was named 'Detoxifier'.

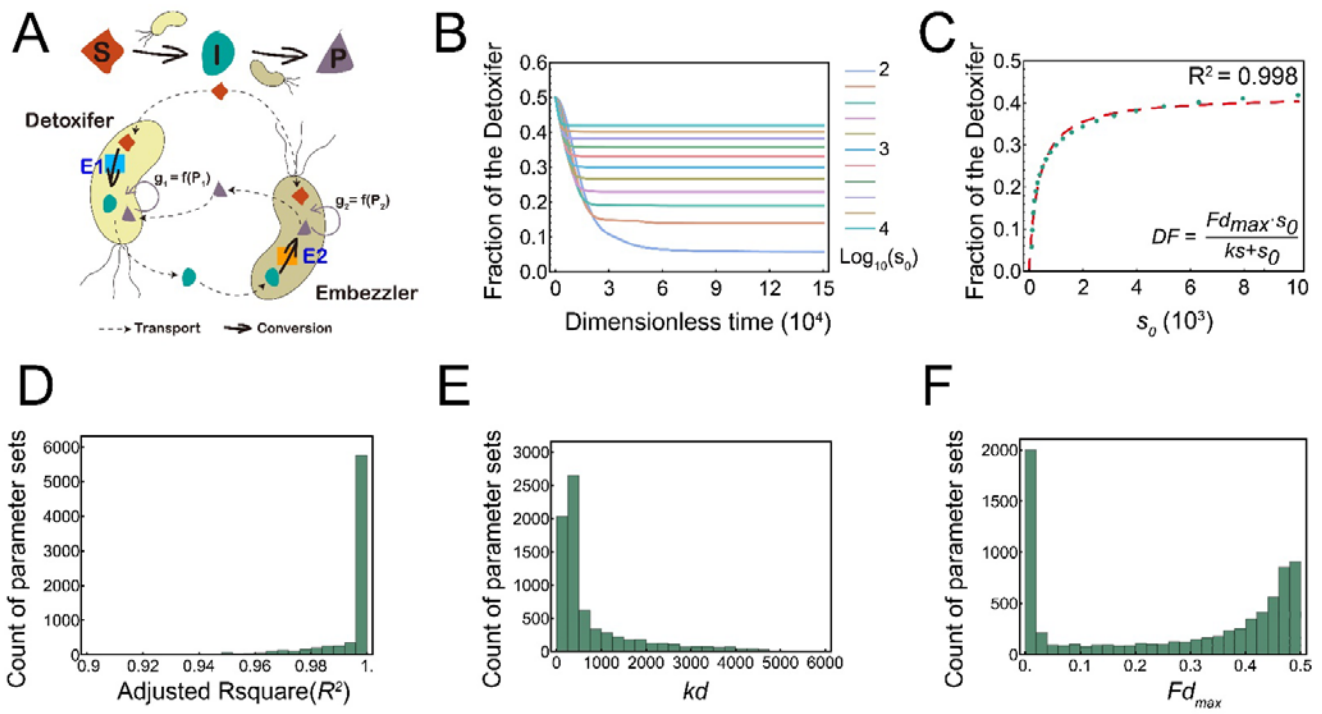

Figure 2 Simulation of the ordinary differential equation (ODE) model excluding substrate toxicity. (A) Schematic diagram showing the basic assumptions of our ODE model without including substrate toxicity. (B-C) A representative case shows how substrate concentration affects the structure of a MDOL community. The simulation dynamics of the fraction of Detoxifier population with the conditions of different initial substrate concentrations are shown in (B). The relationship between substrate concentration and stead-state fraction of Detoxifier is shown in (C).

In (C), the green dots denote the simulated stead-state fraction of Detoxifier, and the red dashed line shows the plot of the best fitting function using Eqn. [1]. Parameter values used in these simulations: $y = 10^{-4}$, $Cp = 10$, $bg = 1$, $a_1 = 10000$, $a_2 = 1000$, $\beta_2 = 1$, $\gamma_s = 1$, $\gamma_i = 1$, $\gamma_p = 1$, $\rho = 10^{-2}$. The best fitting value of *ks* in this case is 35.3, and that of Fd_{max} is 0.417. (D-F) Distributions of Adjusted R^2 (D) of the fitting functions, best fitting value of *ks* (E) and Fd_{max} (F) in the second-round simulations that does not include substrate toxicity, using 7776 parameter value combinations of the five key parameters (a_1, γ_s, γ_i, γ_p, and Cp).

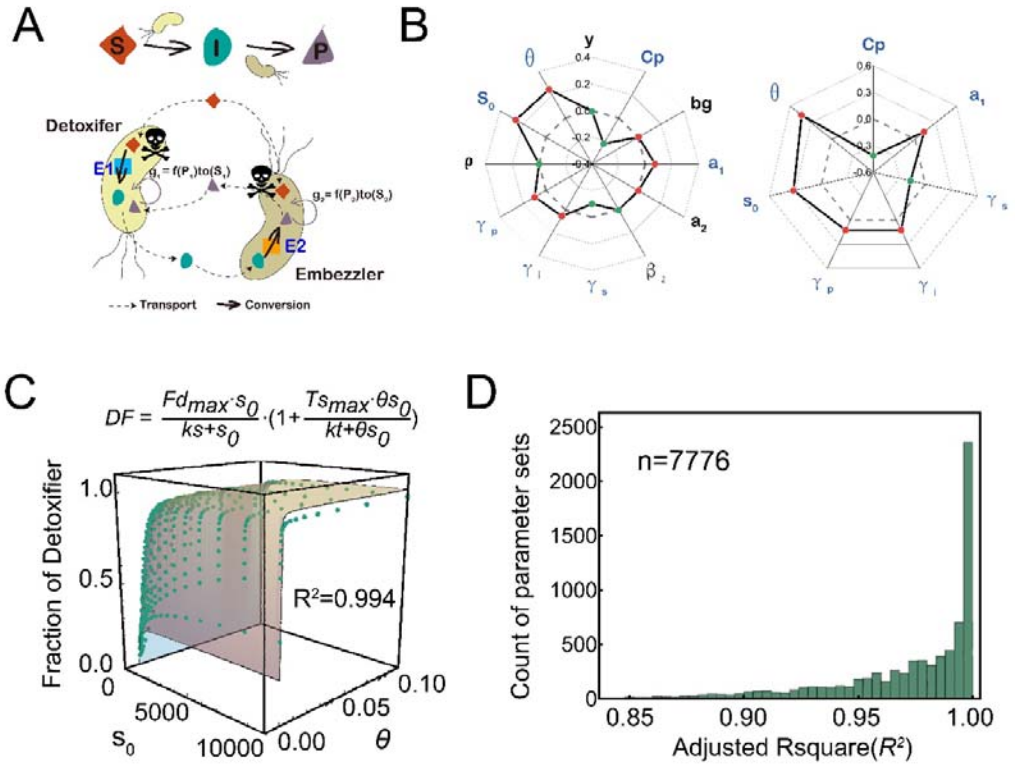

Figure 3 Simulation of the ordinary differential equation (ODE) model that includes substrate toxicity, suggesting that both substrate concentration and its toxicity collectively affect the structure of a community engaged in MDOL. (A) Schematic diagram showing the basic assumptions of our ODE model that includes substrate toxicity. (B) Multiple linear regression analysis of the simulation results of the ODE model showed how the parameters included in the model affect the structure of the MDOL community. Left: results from the first-round simulations that considered all the twelve parameters are shown. Blue font denotes the identified key parameters. Right: results from the second-round simulations that only considered the seven key parameters. The axis of the radar plot denotes the values of fitting coefficients of the parameters from multiple linear regression analyses. Red dots denote the steady-state

fraction of Detoxifier is positively correlated with corresponding parameter, while the green dots represent the negative correlation. The origin axis (0) is highlighted by dash line to emphasize the fact that the closer a value is to zero, the smaller the effect on the community structure by the corresponding parameter. The data are also listed in Supplementary Table 4 and Supplementary Table 5. In this analysis, the toxic effects of substrate on population growth were assumed to follow a reciprocal relationship. Results considering other relationships are shown in Supplementary Figure 3. (C) A representative case shows how both substrate concentration and its toxicity collectively affect the stead-state proportion of Detoxifier cells. The green dots denote the simulated stead-state fraction of Detoxifier, and the surface shows the plot of the best fitting function using Eqn. [2]. Parameter values used in these simulations: $y = 10^{-4}$, Cp = 10, bg = 1, a_1 = 10000, a_2 = 1000, β_2 = 1, γ_s = 1, γ_i =1, γ_p = 1, $\rho = 10^{-2}$. The best fitting value of ks, Fd_{max}, kt, and TS_{max} in this case are 48.9, 0.423, 0.848, 3.39, respectively. (D) Distributions of Adjusted R^2 of the fitting functions in the second-round simulations that includes substrate toxicity, using 7776 parameter value combinations of the five key parameters (a_1, γ_s, γ_i, γ_p, and Cp).

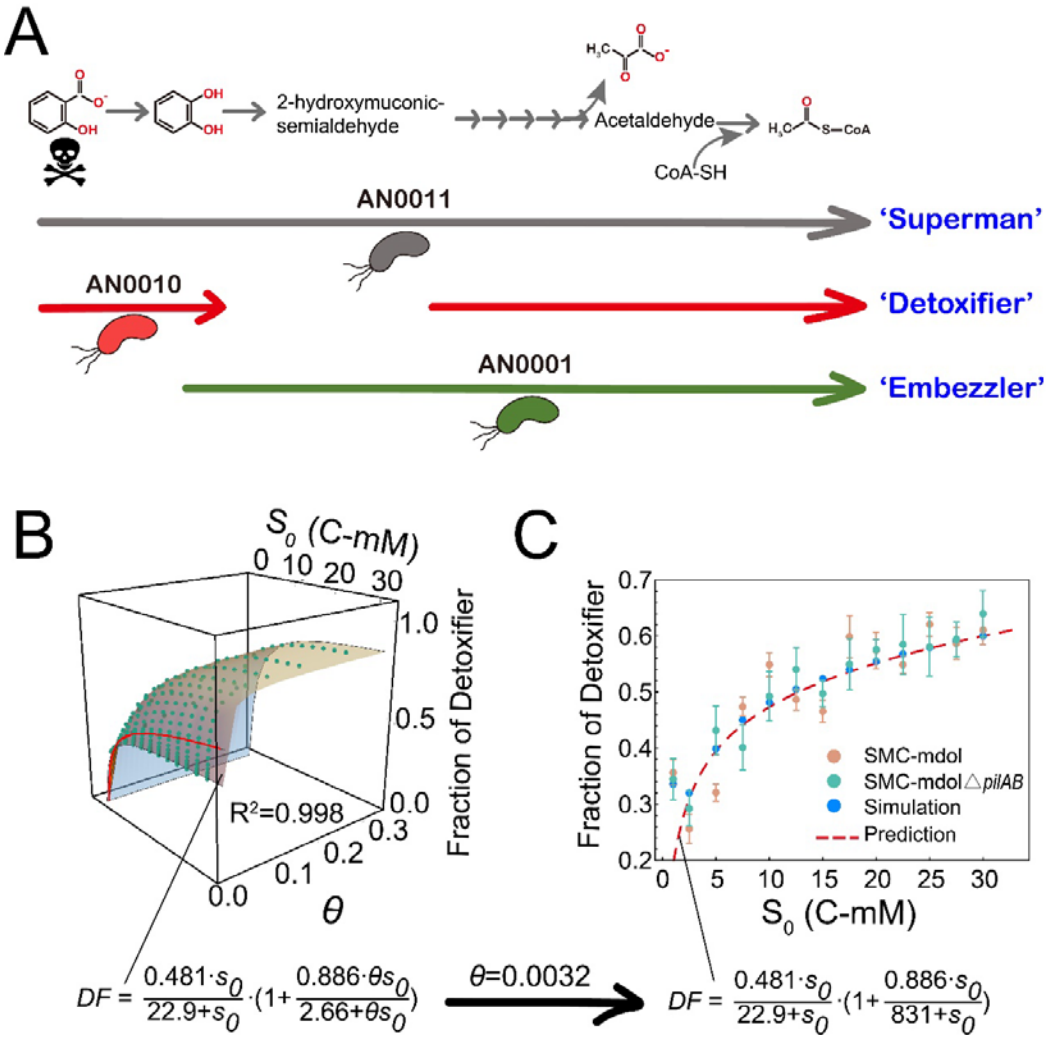

Figure 4 Structure of SMC-mdol in a spatially unstructured system governed by different substrate traits. (A) Design of the SMC-mdol. Shown are the pathway of salicylate degradation in 'Superman' strain *P. stutzeri* AN0011, as well as partial pathways carried out by Detoxifier strain AN0010 and Embezzler strain AN0001. Skull marks that salicylate is toxic. (B) Predicting the structure of the synthetic consortium using our ODE model, as well as the derived predictive function using Eqn. [2]. The relationship between the steady-state fraction of the Detoxifier population and substrate concentration (s_0), as well as substrate toxic strength (θ), was built from our mathematical model using parameters consistent with our

858 experiemental system. Each green dot shows the steady-state fraction of Detoxifier
859 obtained by one simulation accociated with the specific parameter set. The surface
860 diagram shows distribution of the steady-state fraction of Detoxifier predicted by our
861 proposed simple formula. The Red line in the surface denotes the scenarios θ=0.0032,
862 which is the toxic strength of salicylate obtained from experiemental measurements.
863 (C) The experimental measured steady-state fractions of Detoxifier in cultures with
864 different salicylate concentrations is consistent with those from mathematical
865 predictions. Note that in the plots, substrate concentrations are shown in dimentional
866 form (S_0, Cmmol/L), but in the predictive functions, the fitting analysis was
867 performed using its dimensionless form (s_0).
868

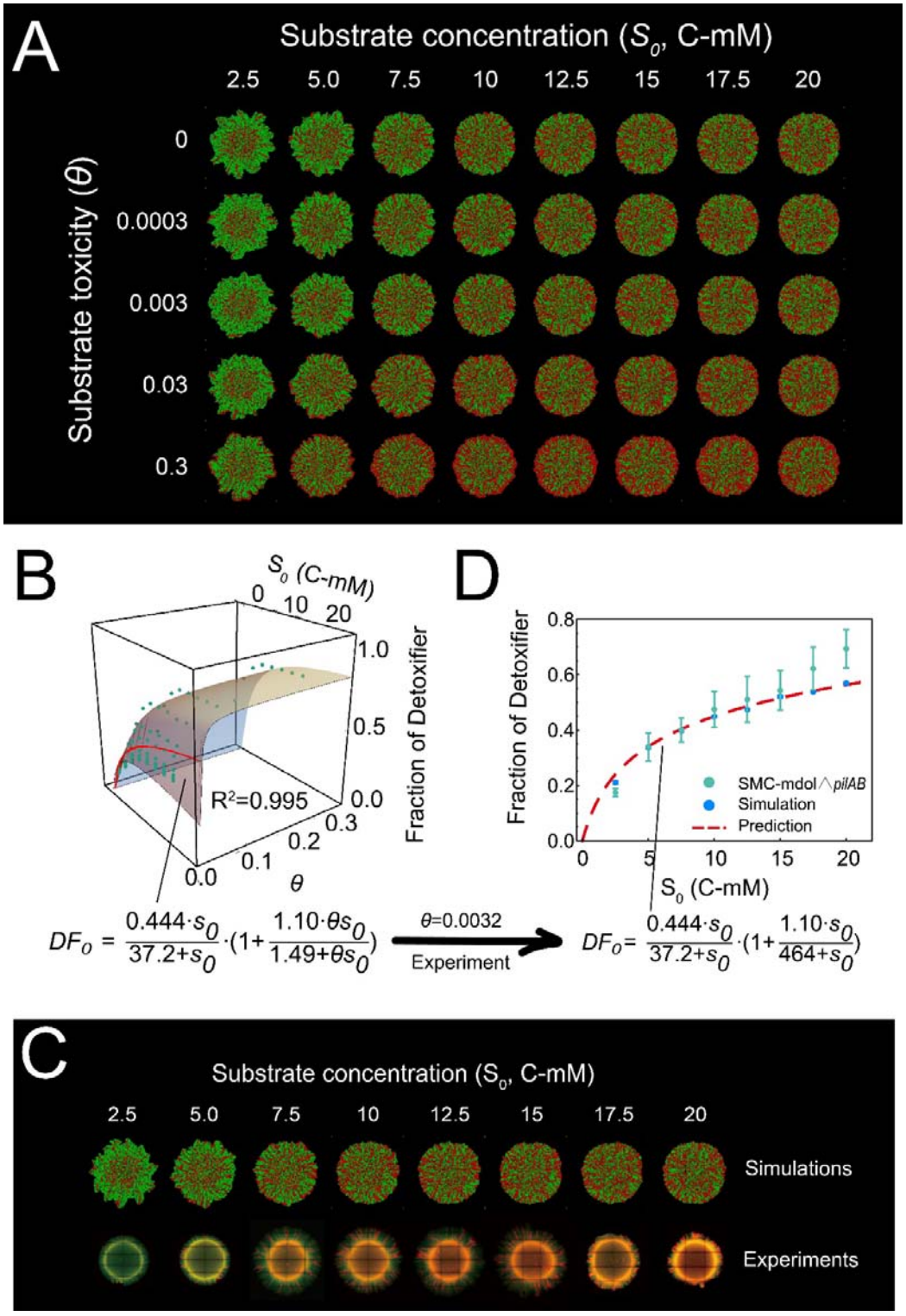

Figure 5 Substrate traits governing the structure of a microbial community engaged in metabolic division of labor (MDOL) in a spatially structured environment. (A) Representative colony patterns from Individual-based (IB) modelling initialized with

different substrate traits. Detoxifier cells are shown in red, while Embezzler cells are shown in green. (B) Analysis of community composition in the expanding region of the colonies from IB simulations across eight kinds of initial substrate concentrations and five different toxic strength. Plot shows how both substrate concentration and its toxicity collectively affect the stead-state proportion of Detoxifier. The green dots denote the simulated stead-state fraction of Detoxifier. The surface shows the plot of the best fitting function using Eqn. [2]. The Red line in the surface denotes the scenarios θ=0.0032, which is the toxic strength of salicylate obtained from experimental measurements. (C) Representative colony patterns from the pattern formation assays of SMC-mdol△*pilAB*, as well as the IB simulations using the parameters matched with our synthetic system (Supplementary Table 7), across eight different initial substrate concentrations. (D) The experimental measured steady-state fractions of Detoxifier in the expanding region of these colonies is consistent with those from mathematical predictions. Note that in the plots, substrate concentrations are shown in dimensional form (S_0, Cmmol/L), but in the predictive functions, the fitting analyses were performed using its dimensionless form (s_0).

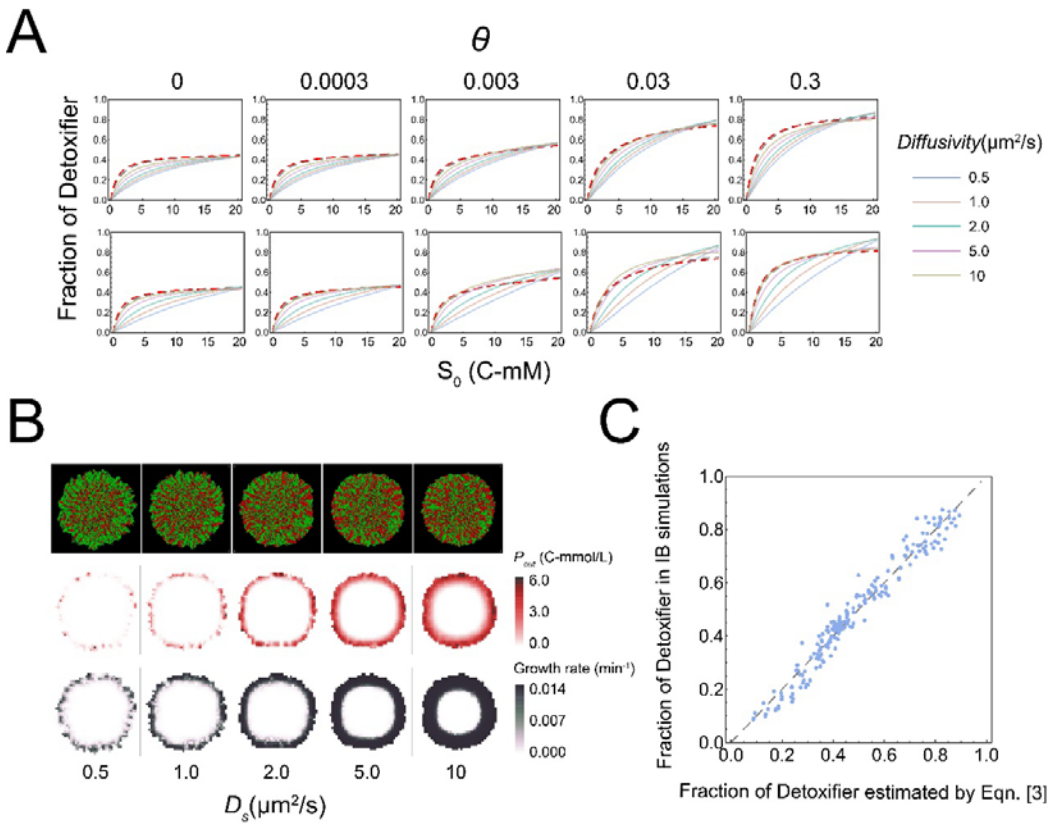

Figure 6 The effects of the diffusion level of substrate, intermediate and product on the structure of MDOL community. (A) The relationship between initial substrate concentration (S_0) with the steady-state proportion of Detoxifier cells in the expanding region of the colonies, across different substance diffusion level (denoted by different curve colors) and different strength of substrate toxicity (θ, denoted by five subgraphs). First row: diffusion levels of S, I and P (that is D_i, D_i, and D_p) were set to be identical and simultaneously modulated in the simulations. Second row: Diffusion levels of I and P (D_i and D_p) were set as default values shown in Supplementary Table 7, while diffusion levels of S were solely modulated. Other parameters in these simulations were initialized with the default values shown in Supplementary Table 7. The simulation data were then fitted to Eqn. [2] to obtain the curves shown in the plot.

The Adjust R^2 values for these fitting analyses range from 0.994 to 0.997. (B) Diffusion levels of substrate affected the thickness of cell 'active layer'. Representative colony images (first row), the corresponding distributions of final product (second row), as well as the distributions of cell growth rates (third row) in the 2D plane at steady-state, obtained from individual-based simulations initialized with different diffusion level of substrate. Shown are the results in which S_0 was set to 10 C-mol/L and θ was 0 (not include substrate toxicity). In the colony images, Detoxifier cells are shown in red, while Embezzler cells are shown in green. Thickness of cell 'active layer' is reflected by thickness of the cell layer that possessing positive growth rate (third row). (C) The linear correlation between the steady-state frequencies of Detoxifier predicted by Eqn. [4] and those frequencies obtained by our Individual-based simulations. The dashed line shows the linear curve in which the predicting results is completely identical to simulated results. The best fitting value of ks, Fd_{max}, kt, TS_{max}, kd_1, and kd_2 in this case are 30.8, 0.446, 1.46, 1.05, 14000, and 44.8 respectively.